RESEARCH ARTICLE SUMMARY

DEVELOPMENTAL BIOLOGY

Assembly of embryonic and extraembryonic stem cells to mimic embryogenesis in vitro

Sarah Ellys Harrison,* Berna Sozen,* Neophytos Christodoulou, Christos Kyprianou, Magdalena Zernicka-Goetz†

INTRODUCTION: Early mammalian development requires the formation of embryonic and extraembryonic tissues and a highly coordinated partnership between them. This close partnership is a prerequisite for successful construction of embryo architecture, with the embryonic tissue generating cells of the embryo proper and the extraembryonic tissues, trophectoderm, and primitive endoderm forming the placenta and the yolk sac. Each of these components and the interactions between them are critical for embryonic development to birth. Embryonic stem cells (ESCs) in culture have the potential to participate in development when introduced into the early embryo. However, when cultured in vitro on their own, they do not recapitulate the spatial and temporal events of early embryogenesis.

RATIONALE: We hypothesized that in order to faithfully model with stem cells the morphogenetic steps involved in mammalian embryogenesis, we would need to establish a developmental dialogue between ESCs and extraembryonic trophoblast stem cells (TSCs) in a three-dimensional (3D) extracellular matrix (ECM) scaffold, to potentially substitute for the basement membrane normally provided by the primitive endoderm.

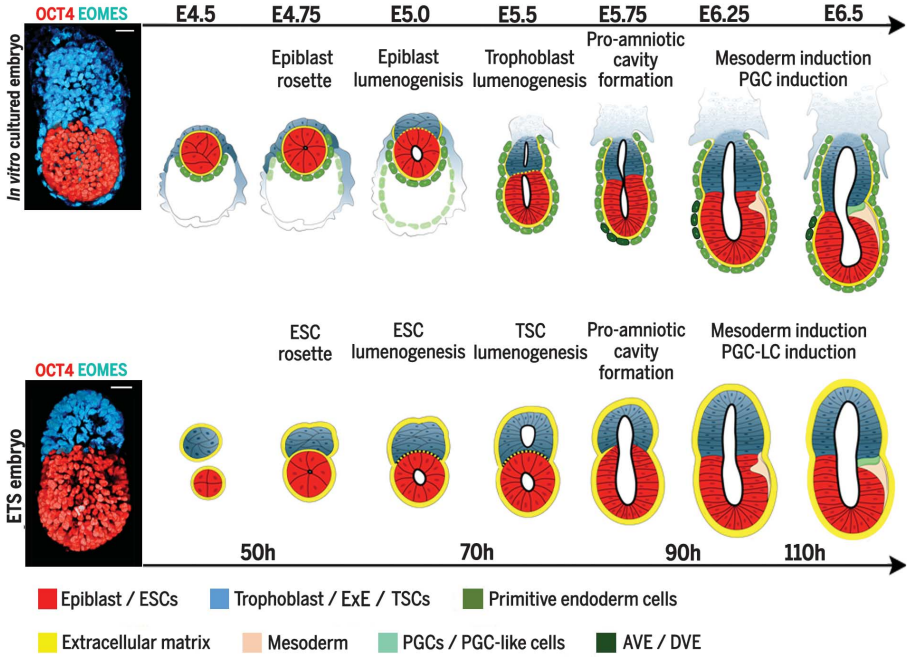

In vitro stem cell-embryos model mouse embryo development from implantation to gastrulation. (**Left**) 3D rendered natural and ETS-embryos. Red, Oct4; cyan, Eomes. (**Right**) Parallel development of natural and ETS-embryos. Red, ESC/epiblast; blue, TSC/trophectoderm/extraembryonic ectoderm cells; green, primitive endoderm/visceral endoderm cells; dark green, distal/anterior visceral endoderm (DVE/AVE); beige, mesoderm cells; pale green, primordial germ cells; yellow line, basement membrane /ECM. Scale bars represent 30 μm.

RESULTS: We combined embryonic and extraembryonic stem cells in vitro on such a 3D matrix and found that these cells were capable of self-assembly into a structure whose development and architecture were similar to that of the natural embryo, leading us to name them in vitro ESC and TSC stem cell–embryos (ETS-embryos). By building ETS-embryos from genetically modified stem cells and using specific inhibitors, we identify morphogenetic events and signaling pathways involved in these early developmental stages. Furthermore, we show that in vitro stem cell embryogenesis can be broken down into a sequence of key steps from implantation stage to germ layer specification. First is the self-organization of ESCs, which leads to polarization and lumenogenesis of ESC-derived embryonic compartment, followed by cavitation in the TSC-derived extraembryonic compartment. Second is the unification of embryonic and extraembryonic cavities into the equivalent of the embryo's proamniotic cavity. Third is the requirement for a dialogue between embryonic and extraembryonic compartments, involving Nodal signaling, that builds characteristic embryo architecture. Fourth is the patterning of the embryonic compartment, revealed by the localized expression of mesoderm markers at the boundary between embryonic and extraembryonic compartments that, as in the natural embryo, is preceded by and dependent upon Wnt signaling. Fifth is the specification of a small cluster of PGC-like cells at the embryonic and extraembryonic boundary in a bone morphogenetic protein (BMP) signaling–dependent manner. Remarkably, such events in in vitro stem cell embryogenesis occur with very similar spatial and temporal dynamics to those taking place in natural embryogenesis.

ON OUR WEBSITE

Read the full article at http://dx.doi.org/10.1126/science.aal1810

CONCLUSION: In this work, we demonstrate that establishing a close cross-talk between embryonic and extraembryonic stem cells in a 3D ECM scaffold is necessary and sufficient for the self-assembly of a structure that recapitulates many of the key spatial and temporal steps of early mammalian embryogenesis. This in vitro ETS-embryo models embryonic architecture and patterning more accurately than has been possible before using ESCs alone. They also provide a simplified platform to dissect the physical, cellular, and molecular mechanisms mediating the critical cross-talk between embryonic and extraembryonic cells during development, and hence are a powerful tool for the future study of mammalian embryogenesis. ■

The list of author affiliations is available in the full article online.
*These authors contributed equally to this work.
†Corresponding author. Email: mzg@mole.bio.cam.ac.uk
Cite this article as S. E. Harrison *et al.*, *Science* **356**, eaal1810 (2017). DOI: 10.1126/science.aal1810

RESEARCH ARTICLE

DEVELOPMENTAL BIOLOGY

Assembly of embryonic and extraembryonic stem cells to mimic embryogenesis in vitro

Sarah Ellys Harrison,[1]* Berna Sozen,[1,2]* Neophytos Christodoulou,[1] Christos Kyprianou,[1] Magdalena Zernicka-Goetz[1]†

Mammalian embryogenesis requires intricate interactions between embryonic and extraembryonic tissues to orchestrate and coordinate morphogenesis with changes in developmental potential. Here, we combined mouse embryonic stem cells (ESCs) and extraembryonic trophoblast stem cells (TSCs) in a three-dimensional scaffold to generate structures whose morphogenesis is markedly similar to that of natural embryos. By using genetically modified stem cells and specific inhibitors, we show that embryogenesis of ESC- and TSC-derived embryos—ETS-embryos—depends on cross-talk involving Nodal signaling. When ETS-embryos develop, they spontaneously initiate expression of mesoderm and primordial germ cell markers asymmetrically on the embryonic and extraembryonic border, in response to Wnt and BMP signaling. Our study demonstrates the ability of distinct stem cell types to self-assemble in vitro to generate embryos whose morphogenesis, architecture, and constituent cell types resemble those of natural embryos.

Early mammalian development requires the formation of embryonic and extraembryonic tissues and their cooperative interactions. As a result of this partnership, the embryonic tissue, epiblast, will become patterned to generate cells of the future organism. Concomitantly, the extraembryonic tissues, the trophectoderm and primitive endoderm, will form the placenta and the yolk sac. These embryonic and extraembryonic tissues become defined before the embryo implants into the uterus as a result of cellular heterogeneity, polarization, and position, culminating in a blastocyst structure with three distinct cell lineages (*1*).

As the embryo implants, the relatively simple architecture of the blastocyst becomes reorganized in a progressive sequence of spatial and temporal morphogenetic steps into the much more complex architecture of the so-called "egg cylinder" (Fig. 1A, top) (*2*, *3*). This remodeling is triggered by dialog between embryonic and extraembryonic tissues that initiates integrin-mediated signaling, leading the embryonic epiblast cells to polarize, adopt a rosette-like configuration, and then undertake lumenogenesis (*4*). This architectural reorganization of the epiblast is followed by development of the trophectoderm into extraembryonic ectoderm (ExE) that also forms a cavity. Finally, both embryonic and extraembryonic cavities unite to form a single proamniotic cavity, and the embryo visibly breaks its symmetry to initiate mesoderm and primordial germ cell induction (Fig. 1A, top). This key symmetry-breaking event occurs at the boundary between embryonic and extraembryonic tissues and involves Nodal, Wnt, and bone morphogenetic protein (BMP) signaling pathways (*5*–*8*).

As the embryo grows from the blastocyst into the elongated structure of the egg cylinder, the primitive endoderm develops into the visceral endoderm (VE), which becomes regionalized. The distal part of the VE (the distal VE, DVE) expresses inhibitors of the Nodal and Wnt signaling pathways and migrates anteriorly (anterior VE, AVE) to pattern the anterior epiblast (*9*–*11*). At the posterior, a BMP4 signal from the ExE induces the activity of Wnt and Nodal in the adjacent epiblast. Nodal feeds back positively on BMP, which in turn reinforces Wnt, in a self-sustaining interaction loop (*12*–*14*). This specifies posterior identity and therefore defines the location for primitive streak formation and mesoderm induction.

Preimplantation epiblast cells have been established as ESCs that can be maintained indefinitely in culture (*15*, *16*). ESCs retain pluripotency and have the ability to be directed to develop into organoids that present an invaluable system to recapitulate many aspects of organ formation in vitro (*17*–*22*). Embryoid bodies or micropatterned colonies developed from ESCs are also a valuable model for development, as they can be induced to express genes associated with specification of embryonic lineages by using external stimuli (*23*–*26*). However, although such gene expression can be polarized, the structures formed do not follow the spatial-temporal events of embryogenesis and ultimately do not acquire the characteristic architecture of a postimplantation embryo. We hypothesized that this is because in these systems, ESCs develop with a drastically different number and spatial organization of cells and, in addition, lack signals from the extraembryonic tissues that guide embryo development upon implantation. Here we test this hypothesis by taking advantage of our recent understanding of the steps involved in the embryonic–extraembryonic interactions during implantation and early postimplantation development (*4*) and trying to mimic them in stem cells developing in vitro.

Experimental strategy

Our strategy was to attempt to use embryonic and extraembryonic stem cells to replicate the spatial and temporal sequence of events of mouse embryogenesis in vitro (*4*). To achieve this, we used single ESCs and small clumps of TSCs (*27*) and developed a culture system that would enable their interaction within a three-dimensional (3D) scaffold of extracellular matrix (ECM) in a medium whose composition (see materials and methods) allows ESCs and TSCs to codevelop, which we created for this purpose (Fig. 1A, bottom). We hypothesized that a 3D scaffold of ECM in Matrigel would be able to substitute for the primitive endoderm by providing ECM essential for epiblast polarization and lumenogenesis. We found that in these culture conditions, ESCs and TSCs developed into an elongated cylindrical architecture typical of the postimplantation mouse embryo (Fig. 1, B and C, and fig. S1a). Careful examination of morphology, size, cell numbers, and expression of lineage markers revealed discrete ESC- and TSC-derived compartments within a single cylindrical structure with a central cavity that was markedly similar to that of postimplantation embryos developing either in vitro or in vivo (Fig. 1, B to G, and fig. S1, b and c). By determining the expression of a typical primitive endoderm marker, Gata4, we confirmed that the formation of these embryo-like structures did not involve the presence of primitive endoderm (Fig. 1H).

Development of these ESC- and TSC-derived structures was highly reproducible: In a typical 3D culture, 22% of all structures comprised both ESCs and TSCs; 61% were built only from ESCs and 17% only from TSCs (Fig. 1, I and J; $n = 400$). Of all structures comprising ESCs and TSCs, most (92.68%, $n = 88$) had the characteristic cylindrical architecture with single adjoining ESC and TSC compartments, whereas the remaining 7.32% had two ESC compartments occupying polar positions in relation to a single TSC compartment (Fig. 1K). These results indicate that ESCs and TSCs cultured in a 3D scaffold of ECM have the ability to self-assemble an embryo architecture, leading us to term these ESC- and TSC-derived embryos, "ETS-embryos."

Proamniotic cavity formation in ETS-embryogenesis

The first critical morphogenetic event in postimplantation embryogenesis is pro-amniotic cavity

[1]Mammalian Embryo and Stem Cell Group, University of Cambridge, Department of Physiology, Development and Neuroscience, Downing Street, Cambridge CB2 3DY, UK. [2]Department of Histology and Embryology, Faculty of Medicine, Akdeniz University, Antalya, 07070, Turkey.
*These authors contributed equally to this work. †Corresponding author. Email: mzg@mole.bio.cam.ac.uk

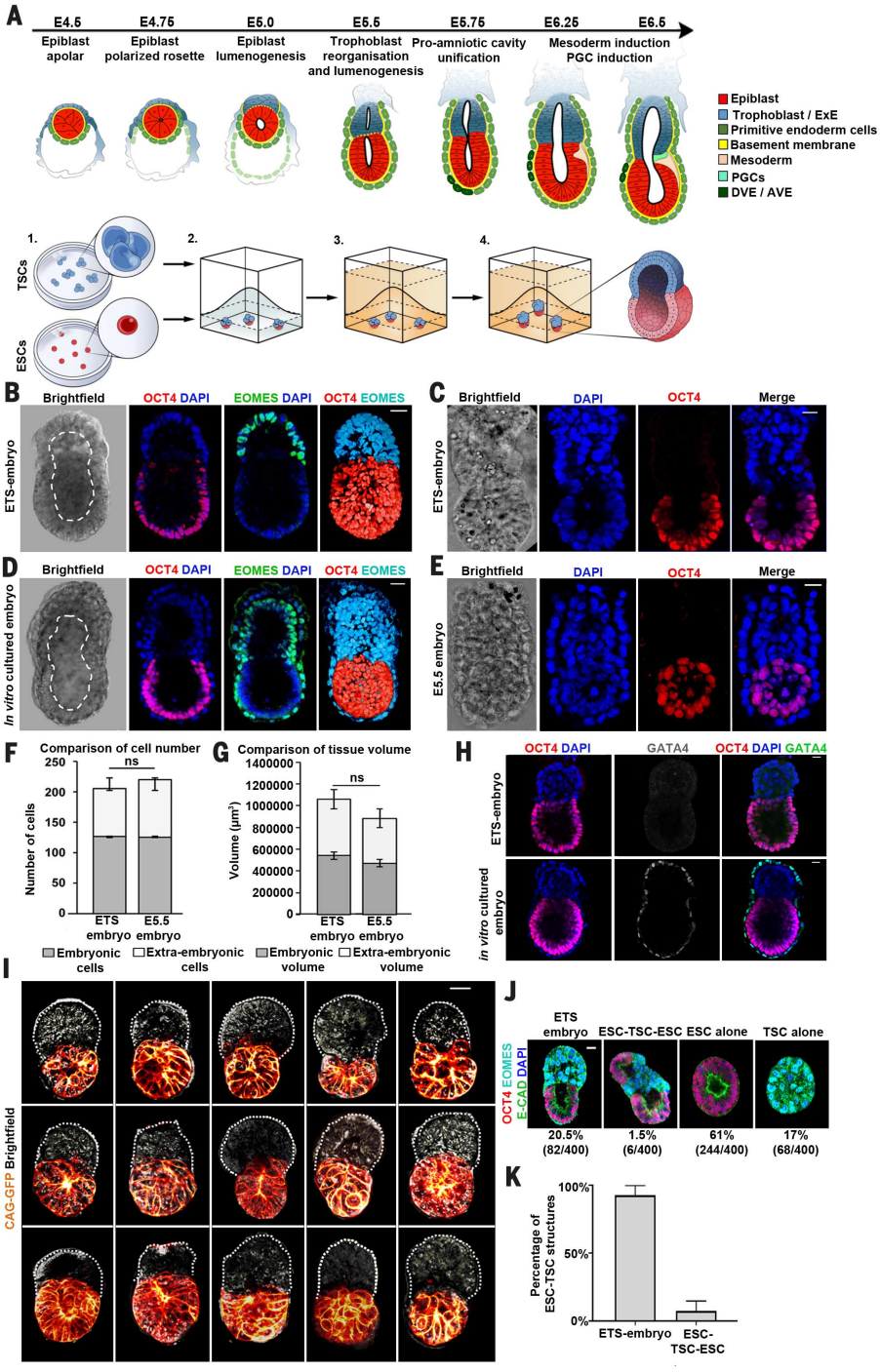

Fig. 1. Self-assembly of ESCs and TSCs into an ETS-embryo. (**A**) Top: Development of the mouse embryo from the preimplantation blastocyst to post-implantation egg cylinder and mesoderm specification. Red cells, epiblast; dark blue cells, trophectoderm/extraembryonic ectoderm; green cells, primitive endoderm/visceral endoderm cells; dark green cells, distal/anterior visceral endoderm; beige cells, mesodermal cells; pale green cells, primordial germ cells; yellow line, basement membrane. Bottom: Scheme of protocol to generate ETS-embryos. ESCs and TSCs cultured in standard conditions (1). Single ESCs and small clumps of TSCs suspended in 3D ECM of Matrigel, plated in drops and allowed to solidify (2), before culturing in ETS-embryo medium established for this purpose [(3); materials and methods). Embryo-like structures emerge within 96 hours (4). (**B**) ETS-embryo of size ~100 μm by 200 μm after 96 hours of culture stained to reveal Oct4 (red) and Eomes (green), embryonic and extraembryonic markers, respectively; DNA, blue. White dashed line highlights cavity. Bar, 30 μm; n = 20. Rightmost panel: 3D rendering of same ETS-embryo: red, Oct4; cyan, Eomes. (**C**) ETS-embryo: Oct4, red; DNA, blue. Bar, 20 μm; n = 20. (**D**) Embryo cultured in vitro for 48 hours from the blastocyst stage: Oct4, red; Eomes, green; DNA, blue. White line highlights cavity. Bar, 30 μm; n = 20. Rightmost panel: 3D rendering of same in vitro–cultured embryo: Oct4, red; Eomes, cyan. (**E**) Postimplantation embryo recovered at E5.5: Oct4, red; DNA, blue. Bar, 20 μm; n = 20. (**F**) The number of cells in ETS-embryos after 96 hours is similar to that of natural embryos (cultured for 48 hours from the late blastocyst stage; equivalent to E5.5 embryos) in embryonic and extraembryonic compartments (Student's t test, n = 20 per group, two separate experiments; not significant). Error bars, SEM. (**G**) Mean tissue volumes of embryonic and extraembryonic parts are similar for ETS-embryos after 96 hours and natural embryos cultured for 48 hours in vitro from the late blastocyst stage (equivalent to E5.5 embryos). Student's t test, n = 20 per group, two separate experiments; not significant. Error bars, SEM. The volume occupied by the visceral endoderm was excluded from quantification in natural embryos. See materials and methods for calculation of the volume. (**H**) Upper panels: ETS-embryo stained to reveal Oct4 (red), DNA (blue), and Gata4 (gray or green). Bar, 20 μm. n = 10. Lower panels: In vitro–cultured embryo for 48 hours from the late blastocyst stage: Oct4, red; DNA, blue; Gata4, gray or green. n = 30. Bar, 20 μm. (**I**) Examples of live ETS-embryos generated from one single typical experiment using CAG-GFP ESCs (*60*) to mark embryonic compartment and wild-type TSCs after 96 hours. Orange, CAG-GFP; black, brightfield. Brightfield was false-colored with the "edges" "look-up-table" function in Fiji software. White dotted line marks the outside of the TSC compartment for clarity. Bar, 20 μm. (**J**) Frequency of ETS-embryos, "twin" (ESC-TSC-ESC) structures, and individual TSC or ESC structures in a representative experiment. Red, Oct4; green, E-cadherin; cyan, Eomes; blue, DNA. Bar, 20 μm. A total of 100 structures counted per experiment; four separate experiments. (**K**) Proportion of ESC- and TSC-structures that form ETS-embryos versus "twin structures." n = 88; four separate experiments. Error bars, SEM.

formation. We therefore wished to determine whether a similar morphogenetic event could take place in ETS-embryos. Recently, it has been discovered that during mammalian embryogenesis, the embryonic cavity forms not through cell death, as previously thought, but through apical cellular constriction followed by lumenogenesis (*4*, *28*). To gain insight into the cavitation of ETS-embryos, we examined the localization of a cell adhesion marker (E-cadherin) at sequential time points in development (Fig. 2, A to C, and fig. S2). After 72 hours of plating, only a single cavity could be detected in ETS-embryos, and it was present in the ESC-compartment (Fig. 2A). By 84 hours, one or more small additional cavities developed within the TSC-compartment (Fig. 2B and fig.S2). Finally, by 96 hours, the cavities in ESC and TSC compartments united into a single

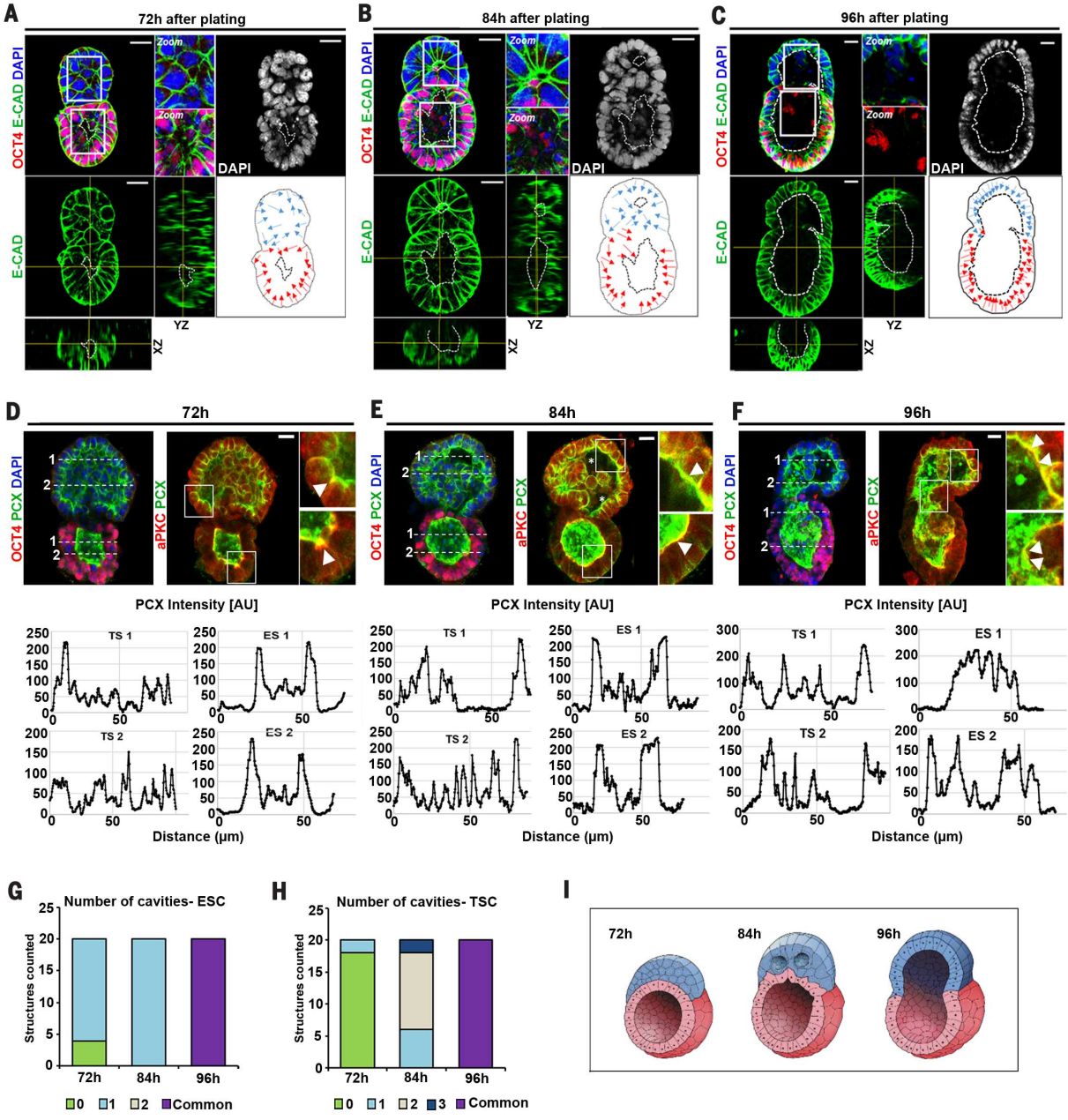

Fig. 2. Morphogenetic steps leading to cavitation of ETS-embryos are similar to those of natural embryos. (**A** to **C**) ETS-embryos after 72, 84, and 96 hours showing progression of cavitation. Oct4, red; E-cadherin, green; DNA, blue or gray. Orthogonal views are shown for E-cadherin staining at each time point. Zoomed fields highlight cavitated areas at each time point; white or black dotted lines highlight cavities. Lower right panel for each time point shows orientation of nuclei in ESC compartments (red) and TSC compartments (blue)—nuclei become aligned to cavities; n = 20 ETS-embryos per time point, at least two separate experiments per time point. Bar, 20 μm. (**D** to **F**) ETS-embryos at three successive time points during cavitation and intensity scans of PCX along the indicated numerically labeled dashed white lines taken at middle z plane. PCX accumulates on the apical sides of cells (marked by aPKC) facing a lumen, so the presence of a cavity is indicated by two strong peaks in the intensity profile. y axis: PCX fluorescence intensity. Staining indicates Oct4/aPKC (red), PCX (green), and DNA (blue). Bar, 20 μm. n = 30, three separate experiments. Zoomed images indicate colocalization of aPKC and PCX (white arrowheads). Asterisks indicate small cavities in the TSC compartment at 84 hours. (**G** and **H**) Quantification of number of cavities in respective ESC- and TSC-compartments of ETS-embryos at 72, 84, and 96 hours. n = 20 ETS-embryos analyzed per time point. (**I**) Schematics depicting "ETS-embryo" morphology during cavitation process at 72, 84, and 96 hours (red, embryonic compartment; blue, extraembryonic compartment).

large cavity (Fig. 2C and fig. S2). These observations demonstrate that a cavity first forms in the ESC-derived embryonic compartment, ahead of cavitation in the TSC-derived extraembryonic compartment, and they finally become united into a single cavity spanning the whole cylindrical structure by 96 hours after stem cell plating (Fig. 2C).

To support these observations, we also examined the distribution of the transmembrane protein Podocalyxin (PCX) together with a marker of apical polarity, atypical protein kinase C (aPKC) (Fig. 2, D to F), in the ESC and TSC compartments of ETS-embryos as their development progressed. PCX is a negatively charged silomucin that accumulates on the apical sides of epiblast cells during proamniotic cavity formation (*4*). In agreement with these observations in embryos, we

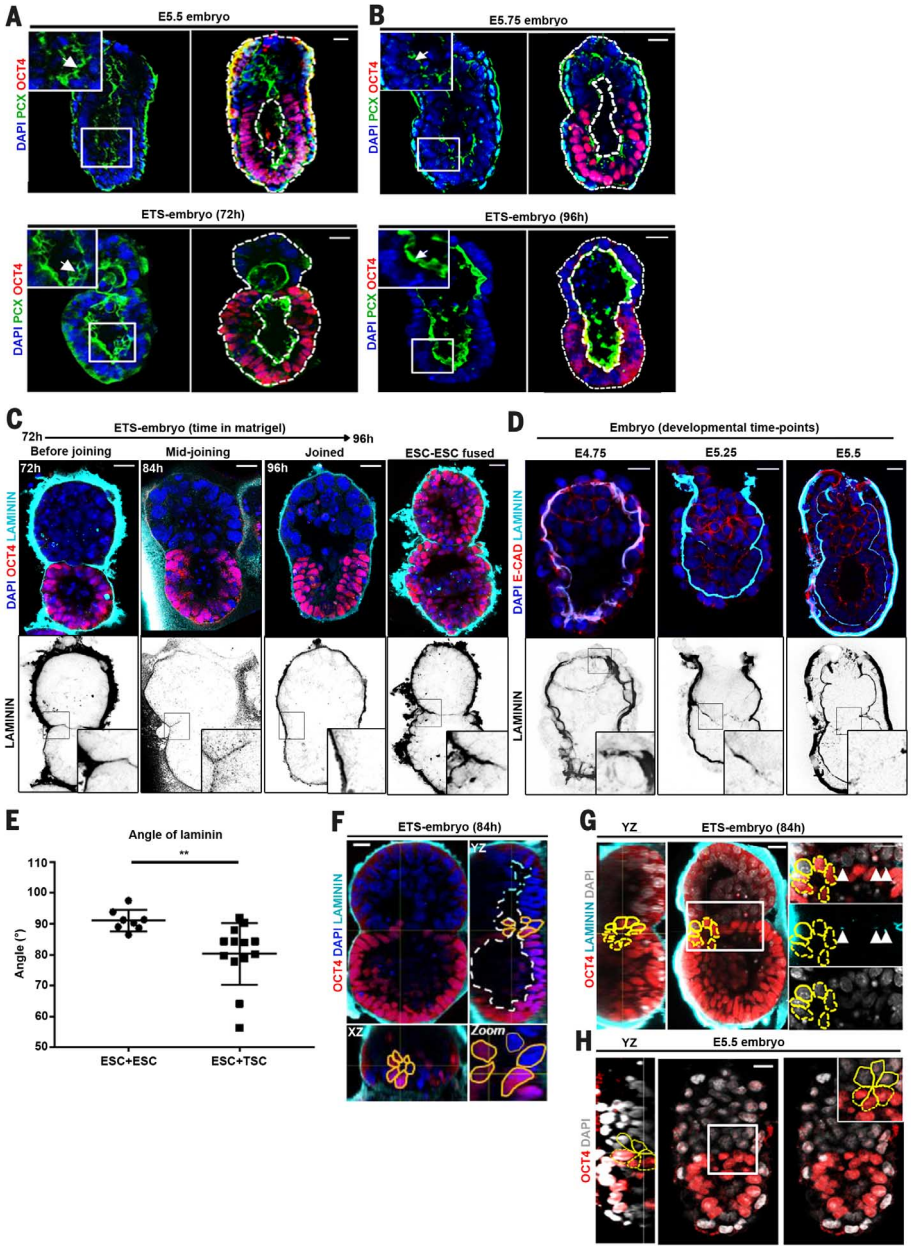

Fig. 3. Morphogenetic rearrangement during cavity unification between embryonic and extra-embryonic compartments. (**A** and **B**) Embryos at E5.5 and E5.75 (upper panels) and ETS-embryos at 72 and 96 hours (lower panels) stained to reveal Oct4 (red), PCX (green), and DNA (blue). Zoomed insets and white arrows highlight cavities; white dashed lines trace outlines of embryo and cavity in respective embryonic or ESC compartments or the common cavity at the later stage. Bar, 20 μm. n = 20 embryos or ETS-embryos each analyzed in at least two separate experiments. (**C**). ETS-embryos during cavitation showing (upper panel) Oct4 (red), DNA (blue), and laminin (cyan). Lower panel shows the laminin staining inverted for better contrast. Black boxes indicate the region of the zoomed inset. Bar, 20 μm; n = 20, two separate experiments. Rightmost panel shows two fused ESC-structures after 84 hours. Inset shows residual laminin that is not broken down between the fusing compartments. n = 8, two separate experiments. (**D**) Peri-implantation embryos showing breakdown of basement membrane between embryonic and extraembryonic compartments; upper panel: E-cadherin (red), DNA (blue), laminin (cyan). Lower panel shows the laminin staining inverted for better contrast. Black boxes indicate the region of the zoomed inset. Bar, 20 μm. n = 10 per stage, two separate experiments. (**E**) Laminin is not displaced from the horizontal in ESC-ESC structures (n = 8, mean angular displacement Θ = 91.05°; pooled from two separate experiments) compared with ETS-embryos (n = 13, mean angular displacement Θ = 80.3°; pooled from two separate experiments). Student's t test, $P < 0.01$, error bars = SEM. For a description of measurement of angular displacement, see materials and methods. (**F**) ETS-embryo during cavitation after 84 hours of culture stained to reveal Oct4 (red), laminin (cyan), DNA (blue). XZ and YZ orthogonal views also shown. Yellow line outlines cells in chimeric arrangements; white dashed lines trace outline of the cavity. Bar, 20 μm. n = 15, two separate experiments. (**G**) Another example of a ETS-embryo during cavitation at 84 hours. Oct4, red; laminin, cyan; DNA, gray. YZ orthogonal view also shown. White arrowheads indicate residual laminin. Yellow lines trace chimeric arrangements of embryonic (dotted) and extraembryonic (solid) cells at boundary; n = 15, two separate experiments. Bar, 20 μm. (**H**) E5.5 embryo. Oct4, red; DNA, gray. YZ orthogonal view also shown. Inset highlights chimeric cell arrangement at the boundary (yellow dotted line, embryonic cells; yellow solid line, extraembryonic cells), n = 10. Bar, 20 μm.

detected the accumulation of PCX along the apical sides of the cells in the ESC compartment when a single lumen was present at 72 hours (Fig. 2, D and G). By contrast, no such accumulation around a cavity was evident in the TSC compartment at this stage (Fig. 2, D and G). By 84 hours, PCX was also seen to accumulate on the apical sides of cells in the TSC compartment as multiple individual cavities emerged in this compartment (Fig. 2, E and H). After 96 hours of development, these ESC and TSC cavities had unified and PCX lined a central, common cavity and was concentrated at the apical sides of cells in both compartments (Fig. 2I, F to I). This sequence of events is similar to proamniotic cavity formation during natural embryogenesis (*4*, *28*). We observed a mean of two dying cells per ESC and TSC compartment, which is similar to the incidence of cell death that we could detect in natural embryos (fig. S3, a to e). The site of cell death in ETS-embryos had no relationship to the ESC or TSC cavitation or ESC-TSC border, suggesting that apoptosis is not a likely driver behind cavity formation and unification, similar to what occurs in natural embryogenesis (fig. S3, a to e).

How the embryonic and extraembryonic cavities unite during embryo development is currently unknown (*4*). Encouraged by our finding of a similar distribution of PCX during natural and ETS-embryogenesis at the time of cavity formation and unification (Fig. 3, A and B), we sought to use the ETS-embryo model to gain insight into how a cavity might develop at the embryonic-extraembryonic interface. Before a continuous cavity formed, the shapes of TSCs at the ESC-TSC border differed noticeably from the columnar morphology of nonborder cells (fig. S4, a and b). Before cavities merged together, a basement membrane (marked by laminin staining) between the compartments was detectable (Fig. 3C, 72 hours, left). This distribution of laminin was similar to that of the basement membrane present between embryonic and extraembryonic compartments of the embryonic day 4.75 (E4.75) embryo (Fig. 3D, left and inset). As ETS-embryos

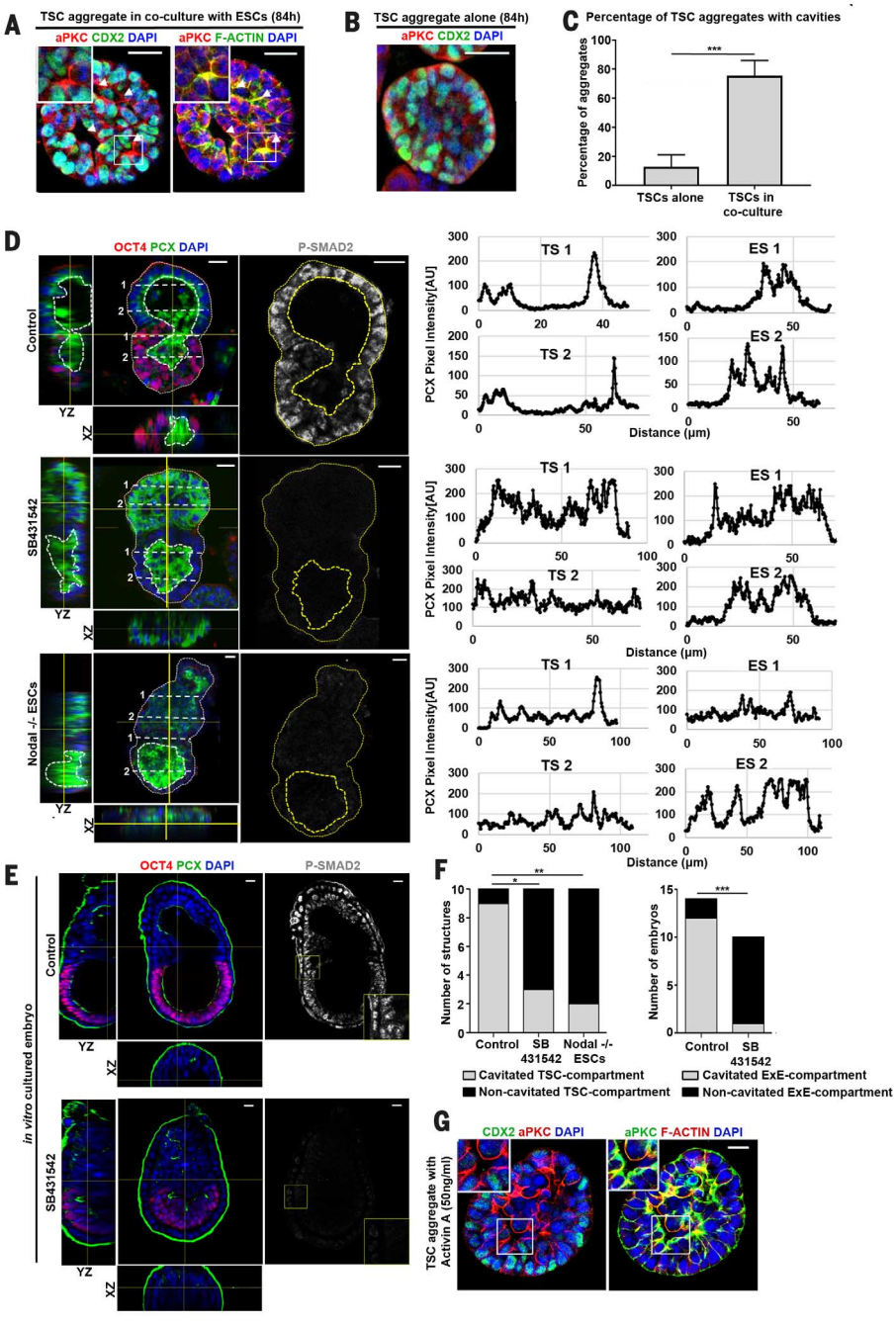

Fig. 4. Cavitation of the TSC compartment requires Nodal/Activin signaling. (**A**) TSC aggregate at 84 hours in coculture but not in contact with ESCs. Cdx2, green; DNA, blue; aPKC, red (left panel) and F-actin, green; DNA, blue; aPKC, red (right panel). White arrowheads indicate cavities. Zoomed inset displays a small cavity opening at a point of aPKC and F-actin enrichment. Bar, 30 μm. $n = 20$, two separate experiments. (**B**) Sole TSC aggregate in 3D Matrigel at 84 hours. Cdx2, green; DNA, blue; aPKC, red. No cavities could be detected and aPKC is not polarized. $n = 20$ structures analyzed that all displayed this morphology, two separate experiments. Bar, 30 μm. (**C**) Quantitation of cavitation in TSC- aggregates cultured either alone or in the presence of ESCs for 84 hours. $n = 10$ structures counted per condition per experiment; two separate experiments. Student's t test, $P < 0.001$. (**D**) ETS-embryos built from either control or *Nodal*$^{-/-}$ ESCs or cultured in 10 μM SB431542 for 96 hours: Oct4, red; PCX, green; DNA, blue; P-SMAD2, gray. Bar, 20 μm. White and yellow dashed lines highlight outline of ETS-embryo and cavity. XZ and YZ orthogonal views highlight cavity where present. Fluorescence traces are of PCX intensity along region indicated by the numbered dotted lines in the ESC and TSC compartments. $n = 10$. (**E**) Embryos recovered at E5.0 and cultured in vitro for 36 hours in control (dimethyl sulfoxide; $n = 14$, three separate experiments) or in the presence of SB431542 (10 μM; $n = 10$, three separate experiments). Oct4, red; PCX, green; DNA, blue; P-SMAD2, gray. Inset highlights P-SMAD2 staining in the extraembryonic ectoderm in each case. Bar, 50 μm. (**F**) Left panel: Quantification showing the number of ETS-embryos with cavitated TSC compartments after 96 hours in culture in control, SB431542, and *Nodal*$^{-/-}$ ESC conditions. $n = 10$ per group, two separate experiments. Count data are presented as a bar chart, and a contingency table was used to perform the statistical test. Fisher's exact test, $P < 0.05$. Right panel: Quantification showing the number of embryos with cavitated extraembryonic compartments when recovered at E5.0 and cultured for 36 hours in control ($n = 14$) or SB431542 ($n = 10$) conditions, two separate experiments. Count data are presented as a bar chart, and a contingency table was used to perform the statistical test. Fisher's exact test, $P < 0.001$. (**G**) TSC aggregate cultured in Activin A (50 ng/ml) for 72 hours. (Left panel) Cdx2, green; DNA, blue; aPKC, red. (Right panel) F-actin, green; DNA, blue; aPKC, red. Zoomed inset displays small cavity opening where aPKC and F-actin are enriched. Bar, 50 μm. $n = 20$, three separate experiments.

underwent cavitation, the laminin boundary became broken (Fig. 3C, 84 hours; Fig. 3E), which mirrored the breakdown of the basement membrane during egg cylinder morphogenesis in vivo (Fig. 3D, middle). In both the ETS-embryo and the natural embryo, full expansion of the cavity across embryonic and extraembryonic compartments led to the complete disappearance of the basement membrane between compartments (Fig. 3C, 96 hours, and Fig. 3D, right). During ETS-embryogenesis, the laminin boundary was displaced toward the TSC compartment, whereas when two structures consisted of only ESCs fused together, laminin was not displaced in any particular direction, suggesting that laminin displacement toward the extraembryonic compartment is a characteristic of the ESC-TSC junction (Fig. 3C, far right, and Fig. 3E). Concomitant with laminin displacement, we also noted formation of rosette-like chimeric cell arrangements comprising both ESCs and TSCs during cavitation of ETS-embryos (Fig. 3, F and G). We found that epiblast and ExE cells adopt very similar cell arrangements at the boundary between compartments in natural embryos (Fig. 3H), which might be involved in the unification of cavities during proamniotic cavity formation. These results reveal the sequence of events leading to embryonic and extraembryonic cavity unification during ETS-embryogenesis and suggest that similar cell rearrangements occur in natural embryogenesis, to facilitate morphogenesis, as also proposed in other models of epithelialization and branching (*29*).

Role of Nodal signaling during ETS-embryogenesis

Although TSCs developing together with ESCs cavitate, the great majority of TSCs developing on their own do not cavitate within the same

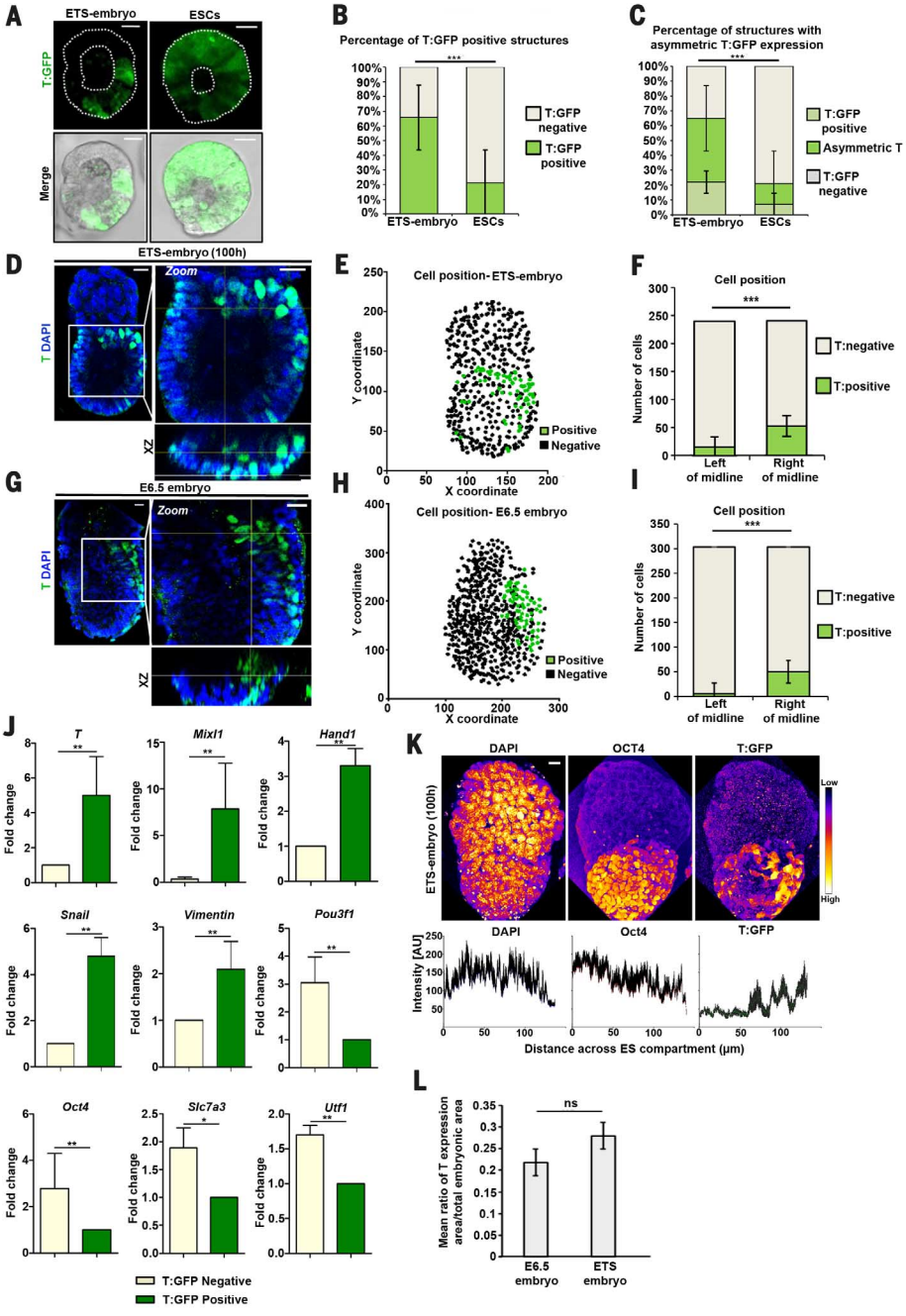

Fig. 5. ETS-embryos develop to express mesoderm markers. (**A**) *T/Brachyury:GFP*-expressing ESCs (green) growing alone (right) or as part of a ETS-embryo (left) in Matrigel. Bar, 20 μm; white dotted lines outline each structure and its cavity. $n = 100$ "ETS-embryos," four experiments; $n = 65$ ESC-alone structures, four experiments. (**B**) Proportion of ETS-embryos expressing *T:GFP* at 96 hours is significantly higher in comparison to ESCs-alone structures. Fisher's exact test, $P < 0.001$, $n = 108$: 64 ETS-embryos and 44 ESC-alone structures counted in two separate experiments. Error bars, SEM. (**C**) Proportion of *T/Brachyury* expressing ETS-embryos or structures comprising only ESCs with asymmetric domain of *T/Brachyury* expression with respect to the long axis (equivalent to the midline) of the structure (materials and methods). Student's *t* test, $P < 0.001$, $n = 100$ ETS-embryos and $n = 100$ structures comprising only ESCs per experiment. Mean of four separate experiments; error bars, SEM. (**D** to **F**) Quantitative assessment of endogenous *T* asymmetry in a ETS-embryo at 100 hours (D) revealing *T* (green) and DNA (blue). Zoomed inset highlights T/Brachyury-expressing region; XZ panel highlights asymmetry in T/Brachyury to one side of structure. Bar, 20 μm. Projection of all cell coordinates in 2D (E): black points, T-negative cells; green points, T-positive cells. Proportion of T-positive versus T-negative cells around mid-line, equivalent to the long axis of each structure [(F); materials and methods]. Fisher's exact test, $P < 0.001$. Error bars, SEM. (**G** to **I**) Quantitative assessment of *T* asymmetry in E6.5 natural embryo (G) revealing T (green) and DNA (blue). Zoomed inset highlights T/Brachyury-expressing region; XZ panel, asymmetry in T/Brachyury. Bar, 20 μm. Projection of cell coordinates (H) as in (E). Proportion of T-positive versus T-negative cells around mid-line, long axis of each structure (I). Fisher's exact test, $P < 0.001$. Error bars, SEM. (**J**) RT-qPCR analysis of the expression of mesodermal markers (*T*, *Mixl1*, and *Hand1*), epithelial-to-mesenchymal transition (EMT) markers (*Snai1* and *Vimentin*), and markers known to be increased in the region opposite to the mesoderm region of the E6.5 embryo (*Pou3f1*, *Oct4*, *Slc7a3*, and *Utf1*) in T:GFP-positive cells of an ETS-embryo (collected after 100 hours in culture) compared with T:GFP-negative cells from the ESC compartment of the same structure. Mesodermal and EMT marker expression was significantly increased in T:GFP-positive cells, whereas cell markers known to be elevated in the region opposite the mesoderm region were significantly decreased. Student's *t* test, $P < 0.05$. $n = 4$ biological replicates. Error bars, SEM. For *Mixl1*, gene expression in some samples of T:GFP-negative cells were undetermined, and so were accepted as zero. (**K**) Top: An ETS-embryo after 100 hours immunostained to reveal DNA (left), Oct4 (middle), and T:GFP (right). Images are maximum projections and are false-colored with the "fire" "look-up table" function in Fiji software to highlight intensity gradients. Bar, 20 μm. Bottom: mean intensity profiles for immunofluorescence stainings plotted as the mean ± SEM for eight different cross sections of the embryonic compartment of the ETS-embryo shown. (**L**) Comparable size of T expression in ETS-embryos and E6.5 embryos. $n = 10$ per group, mean ratio of areas of mesodermal domain/total epiblast in E6.5 embryo. Student's *t* test, not significant; error bars, SEM. For a description of how the ratio was measured and calculated, see materials and methods.

frame of time (Fig. 4, A to C), suggesting that the ESC compartment might signal to promote development of the TSC compartment. One candidate for such signaling would be Nodal/Activin, which is known to be secreted by ESCs (*30*) and to be essential for early postimplantation development (*5*, *31*, *32*). Moreover, Nodal/Activin signaling is required for TSC renewal in culture, and in conventional culture conditions is provided by mouse embryonic fibroblast (MEF) feeder cells or exogenously in the medium (*33*–*35*). Because our culture conditions contain neither of these components, we hypothesized that the ESC compartment might be providing the Nodal/Activin signal required for development of TSCs into the extraembryonic-compartment. Because the earliest role of Nodal signaling is difficult to probe in Nodal knockout embryos owing to the presence of Nodal protein in the reproductive tract (*36*), we used ETS-embryogenesis to gain insight into the role of

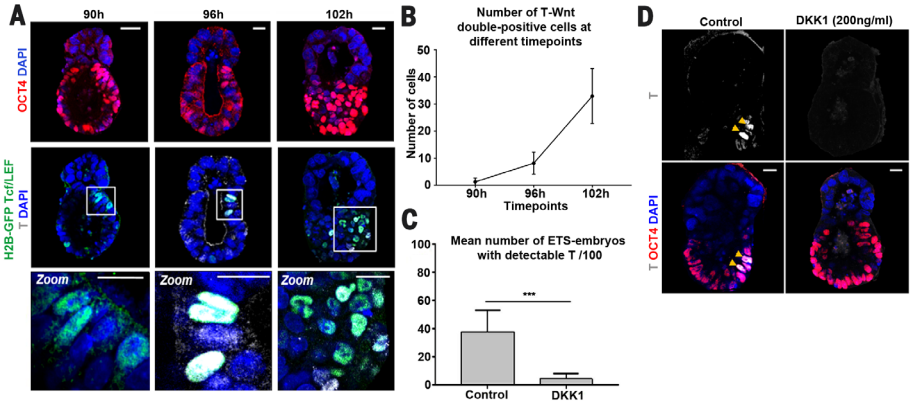

Fig. 6. ETS-embryos express mesoderm markers in response to Wnt signaling. (**A**) ETS-embryos expressing the Wnt reporter H2B-GFP:Tcf/LEF and *T/Brachyury* at 90, 96, and 102 hours of culture. Oct4, red; DNA, blue; H2B-GFP:Tcf/LEF, green; T/Brachyury, white. Bar, 20 μm. Inset (bar, 10 μm) highlights cells coexpressing Wnt reporter and T/Brachyury. $n = 15$ per time point. (**B**) Quantification of mean number of Wnt/Brachyury coexpressing cells detected in the ESC compartment of ETS-embryos with time. The number of cells is significantly different in each group (ANOVA test, $P < 0.01$). $n = 15$ per time point, three separate experiments. Error bars, SEM. (**C**) Proportion of ETS-embryos expressing T/Brachyury is reduced in presence of DKK1 (200 ng/ml) compared to controls. Student's *t* test, $P < 0.001$, $n = 400$, four separate experiments. (**D**) Representative ETS-embryos cultured in DKK1 (200 ng/ml) and control conditions for 96 hours. Oct4, red; DNA, blue; T/Brachyury, white. Yellow arrows indicate T/Brachyury-positive cells in control conditions, undetectable in DKK1 conditions. Bar, 20 μm.

Nodal/Activin in the process of building the embryo-like structure. We generated ETS-embryos in the presence of the Activin/TGF-β (transforming growth factor–β) receptor inhibitor, SB431542 (*37*), which was added to the culture 48 hours after cell plating (Fig. 4D, middle). We verified the inhibition of the Nodal/Activin pathway by assessing phosphorylation of SMAD2 (Fig. 4D, middle), and analyzed PCX staining intensity profiles in different compartments of ETS-embryos to verify cavitation. Although a significant majority of control ETS-embryos developed a cavity in the TSC compartment, in the presence of 10 μm SB431542, the TSC compartment failed to cavitate in a significant majority of ETS-embryos (90% versus 30%, $P < 0.01$, Fisher's exact test; $n = 10$ in both groups, Fig. 4, D and F, left), whereas cavitation within the ESC compartment was unaffected, although we noted a reduction in Oct4 expression (Fig. 4D, middle). To further dissect the role of Nodal/Activin signaling in the development of the TSC compartment, we generated ETS-embryos using tamoxifen inducible-knockout Nodal ESCs (*38*). Similar to the effect of SB431542 treatment, we found that the TSC compartment failed to cavitate in the majority (80%, $P < 0.05$, Fisher's exact test; $n = 10$) of Nodal$^{-/-}$ ESC ETS-embryos (Fig. 4D, bottom, and Fig. 4F, left). Because these results indicated a role of the embryonic compartment and Nodal/Activin signaling in the development of the extraembryonic compartment, we wished to test whether this might also be so in natural embryos. We recovered embryos just before cavitation in the ExE, at E5.0, and cultured them for 36 hours in the presence of 10 μM SB431542 (Fig. 4E bottom). We found that as with ETS-embryos, the ExE in the majority (90%, $P < 0.05$, Fisher's exact test; $n = 10$) of SB431542-treated embryos failed to cavitate, whereas the majority of control embryos cavitated (85%, $P < 0.05$, Fisher's exact test; $n = 14$) (Fig. 4E and 4F, right). Cavitation within the embryonic compartment was unaffected, although there was a reduction in Oct4 expression (Fig. 4E), similar to what we observed in ETS-embryos (Fig. 4D). In agreement with these data, addition of exogenous Activin to TSCs cultured without ESCs allowed cavitation (Fig. 4G; 70%, $P < 0.001$, Fisher's exact test; $n = 20$). Together, these experiments suggest a role of the embryonic compartment, and specifically Nodal/Activin signaling, in supporting the development of the extraembryonic compartment in ETS- and natural embryos developing through early postimplantation stages.

Generation of regionalized mesoderm during ETS-embryogenesis

Once the proamniotic cavity has formed, the next major developmental step is the breaking of the embryo's symmetry to specify the site of germ layer formation. In natural embryogenesis, this is known to involve cooperation between the trophectoderm-derived ExE, which signals development of posterior structures, and the primitive endoderm–derived DVE and AVE, which repress posterior signals (*2*). To determine whether ETS-embryos, which lack DVE and AVE, could initiate an asymmetric expression of germ layer markers, we examined whether they can progress in their development to express *T/Brachyury*, a mesoderm marker (*39*, *40*). In these experiments, we used ESCs that express a *T:GFP* reporter to monitor *T/Brachyury* expression (*41*). We found that from 96 hours of development, the ETS-embryos expressed *T:GFP*, in a domain that was confined to one side of the ESC compartment extending from the boundary with the TSC compartment (Fig. 5A). To address whether this induction of *T:GFP*expression in the ESC compartment was promoted by the neighboring TSC compartment, we also generated structures comprising ESCs only and let them develop under the same conditions and for the same period of time. A significantly higher proportion of ETS-embryos expressed *T:GFP* than the structures composed of only ESCs (Fig. 5, A and B). We also observed that a significantly higher proportion of ESCs developing together with TSCs during ETS-embryogenesis expressed *T:GFP* asymmetrically in comparison to structures composed of only ESCs (Fig. 5C). To quantitatively assess the asymmetry of *T* expression in relation to the axes of the whole structure, we plotted the coordinates of every single cell expressing *T* upon a projection of all cells in the structure and used Fisher's exact test to determine whether a cell's position was related to its propensity to express *T* (Fig. 5, D to F). As a proof-of-principle, we performed similar analyses on E6.5 embryos recovered from the mother (Fig. 5, G to I). Such measurements in both ETS- and natural embryos revealed highly regionalized induction of *T* expression. To confirm the identity of T-expressing cells as mesoderm lineage, we analyzed the expression level of another two mesodermal markers, *Mixl1* and *Hand1*. We found significantly increased expression of transcripts of both of these markers, as well as *T*, in T:GFP-positive cells when compared to T:GFP-negative ESCs at the opposite side of the ETS-embryo (Fig. 5J, top row). These T:GFP-positive cells also expressed elevated levels of the transcription factor *Snai1* and the intermediate filament protein *Vimentin*, which are both expressed in mesenchymal cells, suggesting that cells in the mesodermal region were undergoing cellular changes comparable to those of cells initiating mesoderm formation in the E6.5 embryo (Fig. 5J, middle).

Reverse transcription–quantitative polymerase chain reaction (RT-qPCR) analysis of cells in the ESC compartment opposite the mesodermal region revealed that they expressed markers known to be expressed in the region opposite mesoderm specification in the E6.5 embryo (Fig. 5J, bottom) (*42*, *43*). We also observed an opposing gradient of expression of Oct4 and T:GFP across the embryonic compartment (Fig. 5K), as is known to occur from anterior to posterior in the embryo (*44*). Additionally, the mesodermal region that became specified in ETS-embryos occupied a similar proportion of the ESC-derived embryonic compartment when compared with natural embryos of a comparable stage (Fig. 5L). These results indicate that the TSC compartment can induce regionalized expression of mesoderm markers in a manner mimicking that of the ExE in the embryo.

In normal embryogenesis, Wnt3 expression precedes the induction of mesoderm (*6*). To test whether Wnt signaling might also be required to initiate expression of mesoderm markers in the ETS-embryogenesis, we generated ETS-embryos using H2B-GFP:Tcf/LEF reporter ESCs (*45*) and monitored Wnt signaling activity. After 90 hours,

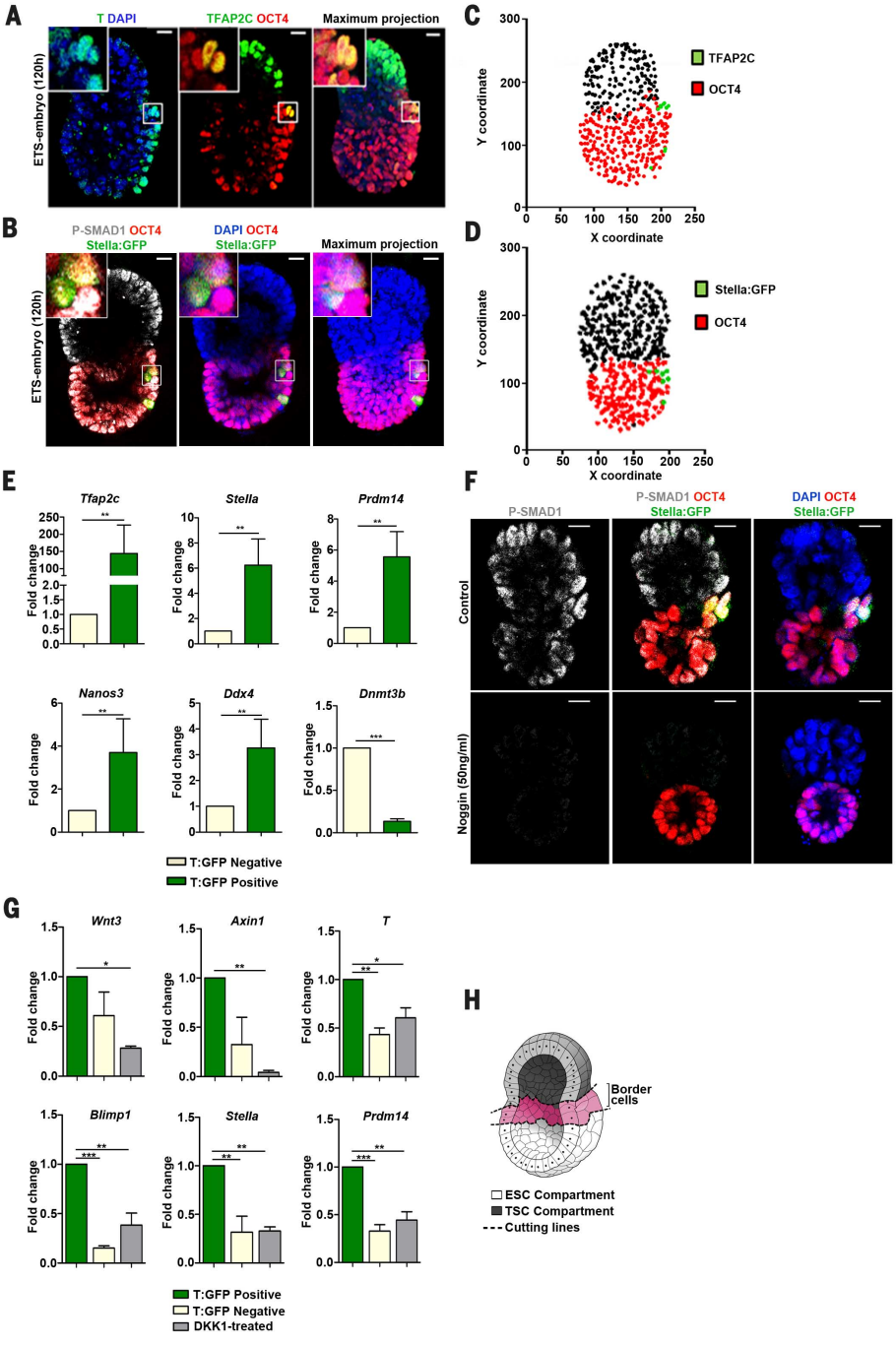

Fig. 7. ETS-embryos express primordial germ cell (PGC) markers in response to BMP signaling. (**A**) ETS-embryo at 120 hours showing asymmetric expression of mesoderm and PGCs markers. Oct4, red; T/Brachyury, green; Tfap2c, green; and DNA, blue. Insets highlight the Oct4-Tfap2c double-positive cells, which occupy the boundary in the T/Brachyury-positive region. Bar, 20 μm. $n = 13$, two separate experiments. Maximum projection shows merge of Tfap2c-Oct4-DAPI. (**B**) ETS-embryo at 120 hours expressing Stella:GFP (green) concomitantly with p-SMAD1 (gray). Oct4, red; DNA, blue. Bar, 20 μm. $n = 15$, three separate experiments. Insets highlight Stella:GFP-positive cells in ESC compartment. Maximum projection shows merge of Stella:GFP-Oct4-DAPI. (**C**) Projected cell coordinates for the same ETS-embryo as in (A): black points, Oct4- and Tfap2c-negative cells; red points; Oct4-positive, Tfap2c-negative cells; green points, Oct4 and Tfap2c double-positive cells. (**D**) Projected cell coordinates for the same ETS-embryo as in (B). Black points, Stella:GFP- and Oct4-negative cells; red points, Oct4-positive and Stella:GFP-negative cells; green points, Oct4- and Stella:GFP-positive cells. (**E**) RT-qPCR analysis of the expression of PGC markers in ETS-embryo. *Tfap2c*, *Stella*, *Prdm14*, *Nanos3*, *Ddx4*, and *Dnmt3b* in T:GFP-positive and T:GFP-negative cells from the same ETS-embryos collected after 120 hours in culture. Expression of PGC markers is significantly increased in T:GFP-positive cells, Student's *t* test, $P < 0.05$. $n = 5$ biological replicates. Error bars, SEM. (**F**) ETS-embryos at 96 hours cultured in control conditions or with BMP antagonist Noggin (50 ng/ml). Oct4, red; DNA, blue; P-SMAD1, gray; Stella-GFP, green. Bar, 20 μm. $n = 15$, two separate experiments. (**G**) RT-qPCR analysis of the expression of PGC markers in "border cells" collected from ETS-embryos in the presence of DKK1 (200 ng/ml) versus T:GFP-positive or -negative cells collected from ETS-embryos in control conditions (collected after 120 hours in culture). Expression of PGC markers (*Blimp1*, *Stella*, and *Prdm14*) is significantly increased in T:GFP-positive cells in control conditions, but this effect is abrogated when DKK1 is introduced into culture conditions . ANOVA followed by Tukey test. $P < 0.05$. $n = 4$ biological replicates. Error bars, SEM. We confirmed inhibition of the Wnt pathway by DKK1 by analysis of the expression of *Axin1*, *Wnt3*, and *T* in all samples. (**H**) Schematic representation of a ETS-embryo (ESC compartment in white and TSC compartment in gray) to illustrate where "border cells" were dissected from in DKK-treated samples for RT-qPCR analysis.

localized expression of H2B-GFP:Tcf/LEF could be detected at the ESC-TSC boundary, but *T/Brachyury* was not expressed at that time (Fig. 6A, left). However, when we cultured ETS-embryos for an additional 6 hours, expression of H2B-GFP:Tcf/LEF colocalized with expression of *T/Brachyury* (Fig. 6A, center). This domain of T/Brachyury and H2B-GFP:Tcf/LEF-expressing cells increased in number and size over the next 6 hours (Fig. 6A, right, and B), indicating that canonical Wnt signaling precedes mesodermal specification. To determine whether Wnt signaling is also essential for mesodermal specification, we generated ETS-embryos and then let them develop in the presence of the canonical Wnt antagonist Dickkopf-related protein–1 (DKK1) (*46*), which was added after 48 hours of culture. In contrast to controls, the proportion of ETS-embryos specifying mesoderm was significantly reduced after 96 hours (38% of controls expressed T, whereas only 4% of structures treated with DKK1 did so, Student's *t* test, $P < 0.001$, $n = 100$; Fig. 6, C and D). These results indicate that Wnt signaling is crucial to induce the expression of mesoderm markers during ETS-embryogenesis, as is the case in natural embryogenesis.

Specification of primordial germ cell–like cells in ETS-embryogenesis

The next major step in embryogenesis is the specification of primordial germ cells (PGCs). In vivo, PGCs are specified at the boundary between embryonic and extraembryonic compartments, at the proximal end of the mesodermal domain (*47*). To test whether ETS-embryogenesis can lead to PGC-like cell specification, we generated ETS-embryos and let them develop beyond mesoderm specification. We then examined expression of several markers, including *Stella*, *Prdm14*, *Tfap2c* (*AP2γ*), *Nanos3*, *Ddx4*, and *Dnmt3b*

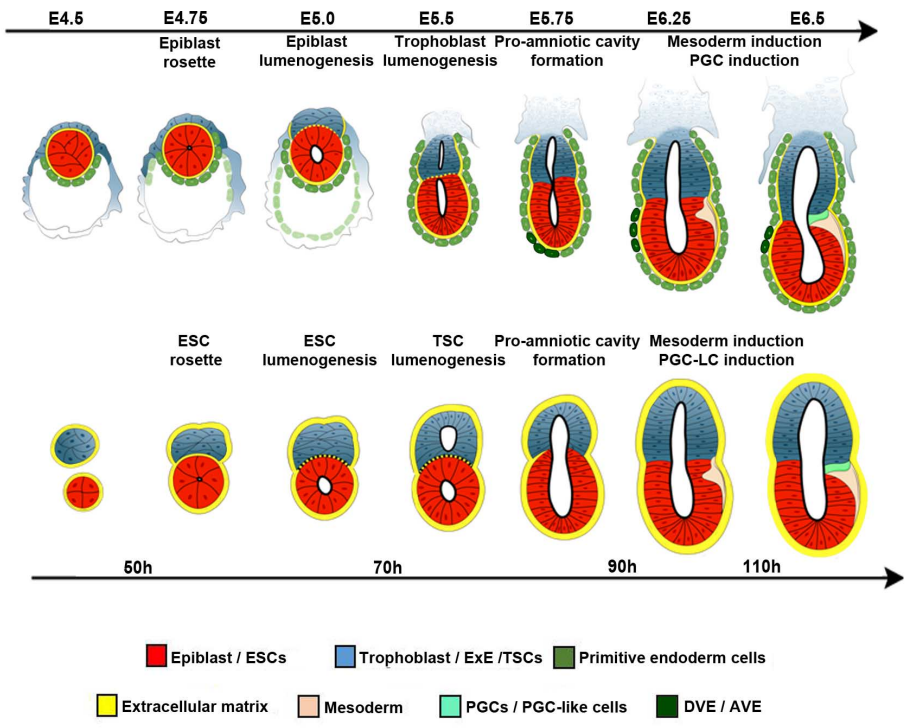

Fig. 8. ETS-embryos as a simplified model of embryo development from the blastocyst stage until mesoderm specification postimplantation. Comparison of development of natural and "ETS-embryos" mouse embryos. Red cells, ESC/epiblast; dark blue cells, TSC/trophectoderm/xtraembryonic ectoderm cells; beige cells, mesoderm cells; pale green cells, primordial germ cells; yellow line, basement membrane/ECM. In the embryo, green cells are primitive endoderm/visceral endoderm cells; dark green cells, distal/anterior visceral endoderm. The ETS-embryo is surrounded by ECM in a manner similar to that of basement membrane of visceral endoderm in natural embryo. Mesoderm-expression domain is similarly positioned and occupies similar area of the embryonic compartment in both ETS-embryos and natural embryos.

(*48*). After 120 hours in culture, we could identify a small cluster of Tfap2c-Oct4 double-positive cells in the ESC compartment, at the ESC-TSC boundary, where *T* was expressed (Fig. 7A). The location of this site is similar to that of PGC formation in vivo (*47*, *48*). To confirm this result, we next generated ETS-embryos using ESCs that express GFP-tagged Stella (*Stella:GFP*) (*49*). In accord with our earlier observations, we found a small domain of Stella:GFP expression after 120 hours in culture (Fig. 7B). To investigate the precise location of these putative-PGC–like cells, we plotted the coordinates of every single cell expressing either of these two PGC markers upon a projection of all cells in the structure. This revealed an average of five Tfap2c-Oct4 double-positive and five Stella:GFP cells at the boundary between the ESC and TSC compartments (Fig. 7, C and D). The precise location of Stella-GFP–positive cells at the boundary between compartments contrasted to that of Stella-GFP expression in structures consisting of ESCs alone, which was distributed in a disorganized manner (fig. S5, a and b). To further investigate gene expression characteristic of PGCs, we collected T:GFP-positive and -negative cells from the ETS-embryos (at the boundary with the extraembryonic compartment) and performed RT-qPCR analysis. This revealed, as expected for PGCs, up-regulated expression of all PGC-marker genes examined—*Tfap2c*, *Stella*, *Prdm14*, *Nanos3*, and *Ddx4*—and down-regulation of *Dnmt3b* when compared with T:GFP-negative cells outside this region (Fig. 7E). These results indicate that ETS-embryos have the potential to specify PGC-like cells at the boundary between embryonic and extraembryonic compartments, as natural embryos.

Specification of PGCs during embryogenesis is induced by BMP signaling from the extra-embryonic compartment (*47*). We therefore hypothesized that BMP signaling might play a similar role in the ETS-embryo model. To test this hypothesis, we first confirmed phosphorylation of SMAD1 in ETS-embryos, as in natural embryos, indicating their competence to specify PGCs (Fig. 7B; Fig. 7F, top; and fig. S6, a and b). We then used ETS-embryogenesis to generate ETS-embryos and let them develop in the presence of Noggin, known to inhibit BMP signaling (*50*), which we confirmed (Fig. 7G). Upon BMP inhibition, a significant majority of ETS-embryos (93%, n = 15) failed to express *Stella:GFP*, in contrast to control ETS-embryos (60%, $P < 0.005$, Fisher's exact test, n = 15; fig. S6c). Finally, we wished to examine whether Wnt signaling is also necessary for induction of expression of PGCs markers during ETS-embryogenesis. To this end, we generated ETS-embryos and treated them with DKK1 (200 ng/ml) after 48 hours of culture. This treatment significantly down-regulated expression of PGC marker genes and *T* in ESC-derived embryonic compartment on the boundary with the TSC-derived compartment, which would undergo PGC specification in control ETS embryos IVEs (Fig. 7, G and H). We verified that the Wnt signaling pathway was down-regulated by analyzing the expression of *Axin1* and *Wnt3* (Fig. 7G). These results indicate that after the induction of expression of mesoderm markers, ETS-embryogenesis progresses to induce expression of PGC markers in a manner similar to that of natural embryogenesis.

Discussion

At the onset of our study, we hypothesized that development of a stem cell model of mammalian embryogenesis might require mimicking the complex spatiotemporal sequence of morphogenetic steps occurring during natural embryogenesis. Our recent work allowed us to reveal the sequence of these morphogenetic steps at the time of implantation and early postimplantation development (*3*, *4*). Here we take advantage of this knowledge and show that by fostering close interactions between embryonic and extraembryonic stem cells in a 3D scaffold of ECM and medium in which they can codevelop, ESCs and TSCs self-assemble into a structure whose development and architecture are very similar to those of the natural embryo. This in vitro embryogenesis can be broken down into a sequence of five key steps in the development of mammalian embryos from implantation stage to germ layer specification: (i) the spontaneous self-organization leading first to polarization and then epithelization and lumenogenesis in the embryonic (ESC) compartment and then cavitation in the extra-embryonic (TSC) compartment; (ii) the unification of embryonic and extraembryonic cavities into the equivalent of the embryo's proamniotic cavity; (iii) the cross-talk between embryonic and extraembryonic compartments, involving Nodal signaling, that builds characteristic embryo architecture; (iv) the self-organization of embryonic and extraembryonic compartments, resulting in asymmetric induction of the localized expression of mesoderm markers at the compartment boundary in a Wnt-dependent manner; and (v) the provision of BMP signaling to specify the PGC-like cells, equivalent to their formation in the embryo. These morphogenetic events follow similar spatiotemporal dynamics during ETS-embryogenesis to those taking place in natural embryogenesis (Fig. 8).

Our studies demonstrate that stem cell–derived ETS-embryos can mimic formation of the embryo's structure and gene expression pattern more accurately than has been possible before with structures derived from ESCs only, such as embryoid bodies (*23*–*26*). There are three critical differences between the ETS-embryos we describe here and embryoid bodies: The former are built from fewer starting numbers of cells to closely resemble cell numbers in the implanting embryo; they are cultured in a 3D scaffold of ECM as epiblast

cells within the embryo; and the ESCs develop in coordination with TSCs as epiblast cells with trophectoderm cells within the embryo. Our previous studies showed that a small number of ESCs cultured in ECM could organize themselves into a rosette that undergoes lumenogenesis in a manner resembling that of the natural embryogenesis (*4*). We show here that these ESC-derived rosettes can develop further to spontaneously—i.e., without provision of a specific external signal—induce mesoderm gene expression. However, we also now show that achieving robust mesoderm induction that respects the embryo's architecture is fostered by the addition of interactions with extraembryonic stem cells.

These results point to a remarkable ability of ESCs to pattern through their interactions with TSCs alone, without a requirement for primitive endoderm–derived structures. This might be because we partially substitute for the primitive endoderm function by providing ECM in the 3D scaffold. In agreement with this hypothesis, we have recently shown that ECM proteins can substitute for primitive endoderm to induce epiblast remodeling at the time of implantation (*4*). However, the induction of asymmetric expression of mesoderm and PGC markers during ETS-embryogenesis was surprising because during natural embryogenesis, primitive endoderm–derived DVE and AVE provide inhibitors to restrict posterior gene expression upon their migration anteriorly (*8*–*11*). The lack of noticeable asymmetry in pSMAD2 in ETS-embryos could be due to the absence of DVE and AVE; nevertheless, our results demonstrate that without the localized provision of antagonists, ETS-embryos break symmetry to induce regionalized, asymmetric expression of mesoderm and PGC markers. We hypothesize that this is either due to a random event or an earlier asymmetric morphogenetic step such as the cell rearrangements that occur during the cavity fusion. Indeed, such rearrangements could potentially reposition signaling receptors to sense and transduce signals from the neighboring compartment not entirely symmetrically. Regardless of the route by which this is achieved, we further hypothesize that secretion of an inhibitory signal might act to restrict mesoderm gene expression in adjacent regions. It will be interesting to further elucidate this process in future and to determine whether incorporating primitive endoderm stem cells (*51*, *52*) into the ETS-embryogenesis model would extend the developmental potential of this model.

In conclusion, we demonstrate that enabling cross-talk between embryonic and extraembryonic stem cells in a 3D ECM scaffold is sufficient to trigger self-organization recapitulating spatiotemporal events that lead to construction of embryo architecture and patterning. This stem cell model of mammalian embryogenesis, in combination with genetic manipulations, might provide a potentially powerful platform to dissect physical and molecular mechanisms that mediate this critical cross-talk during natural embryogenesis.

Materials and Methods

Embryo recovery and culture

Six-week old F_1 female (CBAxC57BL/6) mice were naturally mated and sacrificed at midnight (E5.0) or midday (E5.5) after 5 days postcoitum. The uterus was recovered and embryos were dissected from deciduae in M2 medium and cultured as described previously (*53*). Blastocysts were recovered from the mother at E4.5 by uterine flushing. Recovered blastocysts had their mural trophectoderm dissected away, before plating in μ-plates (Ibidi) and cultured in IVC1 and IVC2 media (Cell Guidance Systems).

Embryo immunostaining

Embryos were fixed in 4% paraformaldehyde for 20 min at room temperature, washed twice in PBT [phosphate-buffered saline (PBS) plus 0.05% Tween-20] and permeabilized for 15 min at room temperature in 0.3% Triton-X-100, 0.1% glycin. Primary antibody incubation was performed overnight at 4°C in blocking buffer [PBS plus 10% fetal bovine serum (FBS), 1% Tween-20]. The next day, embryos were washed twice in PBT, then incubated overnight in secondary antibody in blocking buffer at 4°C. On the third day, embryos were washed twice in PBT and incubated for 1 hour at room temperature in 4´,6-diamidino-2-phenylindole (DAPI) plus PBT (5 mg/ml). Embryos were mounted in DAPI plus PBT before confocal imaging. For antibodies used, see table S1.

Cell culture

ESCs were cultured at 37°C and 5% CO_2 on gelatinized tissue-culture–grade plates and passaged once they reached confluency. Cells were cultured in Dulbecco's modified essential medium (DMEM) with 15% FBS, 2 mM L-glutamine, 0.1 mM 2-mercaptoethanol (2-ME), 0.1 mM nonessential amino acids, 1 mM sodium pyruvate, and 1% penicillin-streptomycin) supplemented with PD0325901 (1 μM), CHIR99021 (3 μM) (2i), and leukemia inhibitory factor (0.1 mM, LIF).

TSCs were cultured at 37°C and 5% CO_2, in RPMI 1640 (Sigma) with 20% FBS, 2 mM L-glutamine, 0.1 mM 2-ME, 1 mM sodium pyruvate, and 1% penicillin-streptomycin, plus FGF4 (Peprotech) and heparin (Sigma) in the presence of inactivated DR4 MEFs (*54*). Cells were passaged at 80% confluency.

Cell lines used in the study

All experiments were performed using E14 or 129 mouse ESCs, CAG-GFP ESCs (*55*), inducible Nodal knockout ESCs (*38*), T:GFP ESCs (*41*), H2B-GFP:Tcf/LEF ESCs (*45*), Stella:GFP ESCs (*49*), and wild-type TSCs.

"3D embedded" culture

ESC colonies were dissociated to single cells, and TSC colonies dissociated into small clumps by incubation with 0.05% trypsin-EDTA at 37°C. Cells were pelleted by centrifugation for 5 min/1000 rpm, washed with PBS, and repelleted. This was repeated twice, then ESC and TSC suspensions were mixed and repelleted. The pellet was resuspended in Matrigel (BD, 356230). The cell suspension was plated on μ-plates (Ibidi) and incubated at 37°C until the Matrigel solidified. Cells were cultured at 37°C and 5% CO_2. ETS-embryo medium was as follows: 50% RPMI, 25% DMEM F-12, and 25% Neurobasal A supplemented with 10% FBS, 2 mM L-glutamine, 0.1 mM 2ME, 0.5 mM sodium pyruvate, 0.25× N2 supplement, 0.5× B27 supplement, or SOS supplement (Cell Guidance Systems Ltd, Cambridge) FGF4 (12.5 ng/ml) and heparin (Sigma) 500 ng/ml (ETS-Embryo medium, ETM, Cell Guidance Systems Ltd., Cambridge). For some experiments, cells were plated by using a 3D "on top" protocol (*56*).

Cell immunostaining

Cells were fixed with 4% paraformaldehyde for 15 min at room temperature, then rinsed twice in PBS. Permeabilization was performed with 0.3% Triton-X-100, 0.1% glycin in PBS for 10 min at room temperature. Primary antibody incubation was performed overnight in blocking buffer (as above) at 4°C. The next day, cells were washed twice in PBS, then incubated overnight in secondary antibody in blocking buffer (as above) at 4°C. DAPI in PBS (5 mg/ml) was added before confocal imaging. For antibodies used, see table S1.

Imaging, processing, and analysis

All images were acquired with a Leica SP5 confocal microscope, using a 40× oil-immersion objective. All analyses were carried out using open-source image analysis software "Fiji" or "Bioemergences" software (*57*).

Estimation of tissue volume

Tissue volume for ETS-embryos and natural embryos was estimated under the assumption that both ETS-embryos and natural embryos were approximately cylinder shaped. The length and radius of each compartment were measured with image analysis software, then the volume of the cylinder was calculated from these measurements as $V = \pi r^2 l$.

Assessment of cells at the embryonic-extraembryonic boundary

Cells were classified as lying on the embryonic-extraembryonic boundary if they had "nearest neighbor" cells within a 20-μm linear distance that were both an ESC and a TSC.

Measurement of laminin displacement angle

Using image analysis software, a line was drawn from ESC compartment to TSC compartment at the middle Z-section of a confocal acquisition of a ETS-embryos. A second line across the boundary was drawn perpendicular. The angle of laminin displacement was then measured relative to these lines. Laminin adjacent to the boundary would therefore have an angle of 90°. Θ is equal to the angle of the laminin extending into the TSC compartment ($\Theta < 90°$).

Assessment of asymmetric gene expression

A line corresponding to the long axis, equivalent to the "midline" of a ETS-embryo (perpendicular

to the embryonic-extraembryonic boundary) was drawn with image analysis software. At each Z-step, the number of cells positioned either side of this line that expressed the marker of interest was counted. If >70% of cells were found to lie on one side of this line, then expression was judged to be asymmetric. In some cases, this method was verified by pointing all cells in a structure using "Bioemergences" image analysis software ("MovIT") and recording their x, y, and z coordinates. Coordinates of cells expressing the marker of interest were also recorded. The long axis, corresponding to the "midline," was determined from the median coordinates in each dimension, and all coordinates data were run through an R script (*58*) that grouped cells according to their position relative to the long axis or midline and whether they expressed the marker of interest. A Fisher's exact test was performed to determine if position relative to the long axis was related to expression of the gene by comparing the distribution of the data to the binomial.

Estimation of proportional area of mesodermal regions in ETS-embryos and E6.5 embryos

Image analysis software was used to measure the area occupied by T-positive, mesodermal cells at the middle Z-section of confocal acquisition data for ETS-embryos and E6.5 embryos. The total area of the embryonic region was also measured in this way in each case. The ratio was calculated as follows: Total area of embryonic region/total area of mesodermal (T-positive) region in each case.

Cell isolation and qRT–PCR

For analysis in fig. S1b, ESC and TSC compartments were collected separately in lysis buffer and RNA was extracted. For analysis of T:GFP-positive cells and opposite T:GFP-negative cells in Fig. 5J and fig. 7, e and g, ETS-embryos were treated briefly with an enzyme-free Hanks'-based cell dissociation buffer for 2 min to remove the Matrigel, then had their TSC-compartment dissected away. The ESC compartment was dissociated to single cells by incubation with 0.05% trypsin-EDTA at 37°C. On average, 15 to 20 GFP-positive and -negative cells were collected separately under a fluorescent microscope and transferred into lysis buffer (Life Technologies). Total RNA was extracted with the Arcturus Pico Pure RNA Isolation Kit, and qRT-PCR was performed with the Power SYBR Green RNA-to-CT 1-Step Kit (Life Technologies) and a Step One Plus Real-time PCR machine (Applied Biosystems). The amounts of mRNA were measured with SYBR Green PCR Master Mix (Ambion). Relative levels of transcript expression were assessed by the ΔΔCt method, with Gapdh as an endogenous control. For qPCR primers used, see table S2.

Statistics

Statistical tests were performed on GraphPad Prism 7.0 software for Windows (*59*). Data were checked for normal distribution and equal variances before each parametric statistical test was performed. If appropriate, data were normalized using a square-root transformation. Where appropriate, t tests were performed with Welch's correction if variance between groups was not equal. Analysis of variance (ANOVA) tests were performed with a Geisser-Greenhouse correction if variance between groups was not equal. Error bars represent SEM in all cases, unless otherwise specified. Figure legends indicate the number of independent experiments performed in each analysis.

REFERENCES AND NOTES

1. C. Y. Leung, M. Zernicka-Goetz, Mapping the journey from totipotency to lineage specification in the mouse embryo. *Curr. Opin. Genet. Dev.* **34**, 71–76 (2015). doi: 10.1016/j.gde.2015.08.002; pmid: 26343010
2. S. J. Arnold, E. J. Robertson, Making a commitment: Cell lineage allocation and axis patterning in the early mouse embryo. *Nat. Rev. Mol. Cell Biol.* **10**, 91–103 (2009). doi: 10.1038/nrm2618; pmid: 19129791
3. I. Bedzhov, S. J. L. Graham, C. Y. Leung, M. Zernicka-Goetz, Developmental plasticity, cell fate specification and morphogenesis in the early mouse embryo. *Philos. Trans. R. Soc. B* **369**, 20130538 (2014). doi: 10.1098/rstb.2013.0538; pmid: 25349447
4. I. Bedzhov, M. Zernicka-Goetz, Self-organizing properties of mouse pluripotent cells initiate morphogenesis upon implantation. *Cell* **156**, 1032–1044 (2014). doi: 10.1016/j.cell.2014.01.023; pmid: 24529478
5. J. Brennan *et al*., Nodal signalling in the epiblast patterns the early mouse embryo. *Nature* **411**, 965–969 (2001). doi: 10.1038/35082103; pmid: 11418863
6. J. A. Rivera-Pérez, T. Magnuson, Primitive streak formation in mice is preceded by localized activation of Brachyury and Wnt3. *Dev. Biol.* **288**, 363–371 (2005). doi: 10.1016/j.ydbio.2005.09.012; pmid: 16289026
7. G. Winnier, M. Blessing, P. A. Labosky, B. L. M. Hogan, Bone morphogenetic protein-4 is required for mesoderm formation and patterning in the mouse. *Genes Dev.* **9**, 2105–2116 (1995). doi: 10.1101/gad.9.17.2105; pmid: 7657163
8. E. J. Robertson, Dose-dependent Nodal/Smad signals pattern the early mouse embryo. *Semin. Cell Dev. Biol.* **32**, 73–79 (2014). doi: 10.1016/j.semcdb.2014.03.028; pmid: 24704361
9. J. A. Belo *et al*., Cerberus-like is a secreted factor with neutralizing activity expressed in the anterior primitive endoderm of the mouse gastrula. *Mech. Dev.* **68**, 45–57 (1997). doi: 10.1016/S0925-4773(97)00125-1; pmid: 9431803
10. M. Yamamoto *et al*., Nodal antagonists regulate formation of the anteroposterior axis of the mouse embryo. *Nature* **428**, 387–392 (2004). doi: 10.1038/nature02418; pmid: 15004567
11. C. Kimura-Yoshida *et al*., Canonical Wnt signaling and its antagonist regulate anterior-posterior axis polarization by guiding cell migration in mouse visceral endoderm. *Dev. Cell* **9**, 639–650 (2005). doi: 10.1016/j.devcel.2005.09.011; pmid: 16256739
12. N. Ben-Haim *et al*., The nodal precursor acting via activin receptors induces mesoderm by maintaining a source of its convertases and BMP4. *Dev. Cell* **11**, 313–323 (2006). doi: 10.1016/j.devcel.2006.07.005; pmid: 16950123
13. P. P. L. Tam, D. A. Loebel, Gene function in mouse embryogenesis: Get set for gastrulation. *Nat. Rev. Genet.* **8**, 368–381 (2007). doi: 10.1038/nrg2084; pmid: 17387317
14. A. Kumar *et al*., Nodal signaling from the visceral endoderm is required to maintain Nodal gene expression in the epiblast and drive DVE/AVE migration. *Dev. Biol.* **400**, 1–9 (2015). doi: 10.1016/j.ydbio.2014.12.016; pmid: 25536399
15. M. J. Evans, M. H. Kaufman, Establishment in culture of pluripotential cells from mouse embryos. *Nature* **292**, 154–156 (1981). doi: 10.1038/292154a0; pmid: 7242681
16. G. R. Martin, Isolation of a pluripotent cell line from early mouse embryos cultured in medium conditioned by teratocarcinoma stem cells. *Proc. Natl. Acad. Sci. U.S.A.* **78**, 7634–7638 (1981). doi: 10.1073/pnas.78.12.7634; pmid: 6950406
17. T. Sato *et al*., Single Lgr5 stem cells build crypt-villus structures in vitro without a mesenchymal niche. *Nature* **459**, 262–265 (2009). doi: 10.1038/nature07935; pmid: 19329995
18. M. Eiraku *et al*., Self-organizing optic-cup morphogenesis in three-dimensional culture. *Nature* **472**, 51–56 (2011). doi: 10.1038/nature09941; pmid: 21475194
19. M. A. Lancaster *et al*., Cerebral organoids model human brain development and microcephaly. *Nature* **501**, 373–379 (2013). doi: 10.1038/nature12517; pmid: 23995685
20. Y. Xia *et al*., The generation of kidney organoids by differentiation of human pluripotent cells to ureteric bud progenitor-like cells. *Nat. Protoc.* **9**, 2693–2704 (2014). doi: 10.1038/nprot.2014.182; pmid: 25340442
21. M. Takasato *et al*., Directing human embryonic stem cell differentiation towards a renal lineage generates a self-organizing kidney. *Nat. Cell Biol.* **16**, 118–126 (2014). doi: 10.1038/ncb2894; pmid: 24335651
22. C. E. Barkauskas *et al*., Type 2 alveolar cells are stem cells in adult lung. *J. Clin. Invest.* **123**, 3025–3036 (2013). doi: 10.1172/JCI68782; pmid: 23921127
23. D. ten Berge *et al*., Wnt signaling mediates self-organization and axis formation in embryoid bodies. *Cell Stem Cell* **3**, 508–518 (2008). doi: 10.1016/j.stem.2008.09.013; pmid: 18983966
24. C. Fuchs *et al*., Self-organization phenomena in embryonic stem cell-derived embryoid bodies: Axis formation and breaking of symmetry during cardiomyogenesis. *Cells Tissues Organs* **195**, 377–391 (2012). doi: 10.1159/000328712; pmid: 21860211
25. S. C. van den Brink *et al*., Symmetry breaking, germ layer specification and axial organisation in aggregates of mouse embryonic stem cells. *Development* **141**, 4231–4242 (2014). doi: 10.1242/dev.113001; pmid: 25371360
26. A. Warmflash, B. Sorre, F. Etoc, E. D. Siggia, A. H. Brivanlou, A method to recapitulate early embryonic spatial patterning in human embryonic stem cells. *Nat. Methods* **11**, 847–854 (2014). doi: 10.1038/nmeth.3016; pmid: 24973948
27. S. Tanaka, T. Kunath, A.-K. Hadjantonakis, A. Nagy, J. Rossant, Promotion of trophoblast stem cell proliferation by FGF4. *Science* **282**, 2072–2075 (1998). doi: 10.1126/science.282.5396.2072; pmid: 9851926
28. M. N. Shahbazi *et al*., Self-organization of the human embryo in the absence of maternal tissues. *Nat. Cell Biol.* **18**, 700–708 (2016). doi: 10.1038/ncb3347; pmid: 27144686
29. A. Villasenor, D. C. Chong, M. Henkemeyer, O. Cleaver, Epithelial dynamics of pancreatic branching morphogenesis. *Development* **137**, 4295–4305 (2010). doi: 10.1242/dev.052993; pmid: 21098570
30. T. Watabe, K. Miyazono, Roles of TGF-beta family signaling in stem cell renewal and differentiation. *Cell Res.* **19**, 103–115 (2009). doi: 10.1038/cr.2008.323; pmid: 19114993
31. D. Mesnard, M. Guzman-Ayala, D. B. Constam, Nodal specifies embryonic visceral endoderm and sustains pluripotent cells in the epiblast before overt axial patterning. *Development* **133**, 2497–2505 (2006). pmid: 16728477
32. A. Camus, A. Perea-Gomez, A. Moreau, J. Collignon, Absence of Nodal signaling promotes precocious neural differentiation in the mouse embryo. *Dev. Biol.* **295**, 743–755 (2006). doi: 10.1016/j.ydbio.2006.03.047; pmid: 16678814
33. M. Guzman-Ayala, N. Ben-Haim, S. Beck, D. B. Constam, Nodal protein processing and fibroblast growth factor 4 synergize to maintain a trophoblast stem cell microenvironment. *Proc. Natl. Acad. Sci. U.S.A.* **101**, 15656–15660 (2004). doi: 10.1073/pnas.0405429101; pmid: 15505202
34. Y. Ohinata, T. Tsukiyama, Establishment of trophoblast stem cells under defined culture conditions in mice. *PLOS ONE* **9**, e107308 (2014). doi: 10.1371/journal.pone.0107308; pmid: 25203285
35. C. Kubaczka *et al*., Derivation and maintenance of murine trophoblast stem cells under defined conditions. *Stem Cell Reports* **2**, 232–242 (2014). doi: 10.1016/j.stemcr.2013.12.013; pmid: 24527396
36. C. B. Park, D. Dufort, Nodal expression in the uterus of the mouse is regulated by the embryo and correlates with implantation. *Biol. Reprod.* **84**, 1103–1110 (2011). doi: 10.1095/biolreprod.110.087239; pmid: 21270430
37. G. J. Inman *et al*., SB-431542 is a potent and specific inhibitor of transforming growth factor-beta superfamily

type I activin receptor-like kinase (ALK) receptors ALK4, ALK5, and ALK7. *Mol. Pharmacol.* **62**, 65–74 (2002). doi: 10.1124/mol.62.1.65; pmid: 12065756
38. Q. Wu *et al*., Nodal/activin signaling promotes male germ cell fate and suppresses female programming in somatic cells. *Development* **140**, 291–300 (2013). doi: 10.1242/dev.087882; pmid: 23221368
39. B. G. Herrmann, Expression pattern of the Brachyury gene in whole-mount TWis/TWis mutant embryos. *Development* **113**, 913–917 (1991). pmid: 1821859
40. D. G. Wilkinson, S. Bhatt, B. G. Herrmann, Expression pattern of the mouse T gene and its role in mesoderm formation. *Nature* **343**, 657–659 (1990). pmid: 1689462
41. H. J. Fehling *et al*., Tracking mesoderm induction and its specification to the hemangioblast during embryonic stem cell differentiation. *Development* **130**, 4217–4227 (2003). doi: 10.1242/dev.00589; pmid: 12874139
42. A. Scialdone *et al*., Resolving early mesoderm diversification through single-cell expression profiling. *Nature* **535**, 289–293 (2016). doi: 10.1038/nature18633; pmid: 27383781
43. G. Peng *et al*., Spatial transcriptome for the molecular annotation of lineage fates and cell identity in mid-gastrula mouse embryo. *Dev. Cell* **36**, 681–697 (2016). doi: 10.1016/j.devcel.2016.02.020; pmid: 27003939
44. H. R. Schöler, G. R. Dressler, R. Balling, H. Rohdewohld, P. Gruss, Oct-4: A germline-specific transcription factor mapping to the mouse t-complex. *EMBO J.* **9**, 2185–2195 (1990). pmid: 2357966
45. A. Ferrer-Vaquer *et al*., A sensitive and bright single-cell resolution live imaging reporter of Wnt/ß-catenin signaling in the mouse. *BMC Dev. Biol.* **10**, 121 (2010). doi: 10.1186/1471-213X-10-121; pmid: 21176145
46. A. Niida *et al*., DKK1, a negative regulator of Wnt signaling, is a target of the beta-catenin/TCF pathway. *Oncogene* **23**, 8520–8526 (2004). doi: 10.1038/sj.onc.1207892; pmid: 15378020
47. K. A. Lawson *et al*., Bmp4 is required for the generation of primordial germ cells in the mouse embryo. *Genes Dev.* **13**, 424–436 (1999). doi: 10.1101/gad.13.4.424; pmid: 10049358
48. U. Günesdogan, E. Magnúsdóttir, M. A. Surani, Primordial germ cell specification: A context-dependent cellular differentiation event. *Philos. Trans. R. Soc. Lond. B Biol. Sci.* **369**, 20130543 (2014). doi: 10.1098/rstb.2013.0543; pmid: 25349452
49. B. Payer *et al*., Generation of stella-GFP transgenic mice: A novel tool to study germ cell development. *Genesis* **44**, 75–83 (2006). doi: 10.1002/gene.20187; pmid: 16437550
50. L. B. Zimmerman, J. M. De Jesús-Escobar, R. M. Harland, The Spemann organizer signal noggin binds and inactivates bone morphogenetic protein 4. *Cell* **86**, 599–606 (1996). doi: 10.1016/S0092-8674(00)80133-6; pmid: 8752214
51. T. Kunath *et al*., Imprinted X-inactivation in extra-embryonic endoderm cell lines from mouse blastocysts. *Development* **132**, 1649–1661 (2005). doi: 10.1242/dev.01715; pmid: 15753215
52. K. K. Niakan, N. Schrode, L. T. Y. Cho, A.-K. Hadjantonakis, Derivation of extraembryonic endoderm stem (XEN) cells from mouse embryos and embryonic stem cells. *Nat. Protoc.* **8**, 1028–1041 (2013). doi: 10.1038/nprot.2013.049; pmid: 23640167
53. I. Bedzhov, C. Y. Leung, M. Bialecka, M. Zernicka-Goetz, *In vitro* culture of mouse blastocysts beyond the implantation stages. *Nat. Protoc.* **9**, 2732–2739 (2014). doi: 10.1038/nprot.2014.186; pmid: 25356584
54. S. Tanaka, Derivation and culture of mouse trophoblast stem cells in vitro. *Methods Mol. Biol.* **329**, 35–44 (2006). pmid: 16845982
55. J. M. Rhee *et al*., *In vivo* imaging and differential localization of lipid-modified GFP-variant fusions in embryonic stem cells and mice. *Genesis* **44**, 202–218 (2006). doi: 10.1002/dvg.20203; pmid: 16604528
56. G. Y. Lee, P. A. Kenny, E. H. Lee, M. J. Bissell, Three-dimensional culture models of normal and malignant breast epithelial cells. *Nat. Methods* **4**, 359–365 (2007). doi: 10.1038/nmeth1015; pmid: 17396127
57. E. Faure *et al*., A workflow to process 3D+time microscopy images of developing organisms and reconstruct their cell lineage. *Nat. Commun.* **7**, 8674 (2016). pmid: 26912388
58. R Core Team, R: A language and environment for statistical computing. R Foundation for Statistical Computing, Vienna, Austria. www.R-project.org/.
59. GraphPad Prism version 7.00 for Windows, GraphPad Software, La Jolla, CA; www.graphpad.com.
60. J. M. Rhee *et al*., In vivo imaging and differential localization of lipid-modified GFP-variant fusions in embryonic stem cells and mice. *Genesis* **44**, 202–218 (2006). doi: 10.1002/dvg.20203; pmid: 16604528

ACKNOWLEDGMENTS

We are grateful to D. Glover, M. Shahbazi, S. Vuoristo, and F. Antonica for helpful feedback on the manuscript; A. Hupalowska for drawing models (Figs. 1A, 2I, and 8) and G. Recher for 3D rendering (Fig. 1, B and D); the creators of the "Bioemergences" platform for providing image analysis tools; and V. Kuskoff, A. Surani, and B. Herrmann for providing T:GFP ESCs and Stella:GFP ESCs. We are grateful to the Wellcome Trust and ERC for supporting this work. S.E.H. and C.K. are both supported by Biotechnology and Biological Sciences Research Council doctoral training partnership studentships. B.S. is supported by the International Research Fellowship Program 2214/A from Scientific and Technological Research Council of Turkey, and M.Z.-G. by the Wellcome Trust. S.E.H. served as an intern in the Cambridge, UK, office of *Science*/AAAS. M.Z.-G. and S.E.H. are inventors on a patent application (1615343.9) submitted by Cell Guidance Systems, in which the University of Cambridge and the Wellcome Trust are beneficiaries, that covers the method and medium composition used to generate "stem cell–derived embryos." S.E.H. and B.S. carried out experiments and data analysis on ETS-embryos. N.C. and C.K. carried out experiments on natural embryos. M.Z.-G. conceived and supervised the study and wrote the paper with the help of S.E.H. and B.S.

SUPPLEMENTARY MATERIALS

www.sciencemag.org/content/356/6334/eaal1810/suppl/DC1
Figs. S1 to S6
Tables S1 and S2

9 October 2016; accepted 17 February 2017
Published online 2 March 2017
10.1126/science.aal1810

Editor's Summary

In vitro embryogenesis

Pluripotent embryonic stem cells (ESCs) can differentiate into any adult cell type; however, aggregates of these cells do not mimic embryonic architecture when grown in culture. To see whether mouse ESCs and their extraembryonic counterparts, trophoblast stem cells (TSCs), can recapitulate normal development, Harrison *et al.* combined ESCs and TSCs in an extracellular matrix culture (see the Perspective by Pera). The resultant "ETS-embryos" displayed considerable resemblance to normal embryos, even specifying mesoderm and primordial germ cells at the boundary between embryonic and extraembryonic compartments. These ETS-embryos are a genetically tractable tool for studying mammalian embryogenesis.

Science, this issue p. eaal1810; see also p. 137